Clocking the Melting Transition of Charge and Lattice Order in $1T$-TaS_2 with Ultrafast Extreme-Ultraviolet Angle-Resolved Photoemission Spectroscopy

J. C. Petersen,[1,2] S. Kaiser,[2] N. Dean,[2] A. Simoncig,[2] H. Y. Liu,[2] A. L. Cavalieri,[2] C. Cacho,[3] I. C. E. Turcu,[3] E. Springate,[3] F. Frassetto,[4] L. Poletto,[4] S. S. Dhesi,[5] H. Berger,[6] and A. Cavalleri[1,2]

[1]*Department of Physics, Oxford University, Clarendon Laboratory, Oxford, United Kingdom*
[2]*Max Planck Research Department for Structural Dynamics, University of Hamburg, Centre for Free Electron Laser Science, Hamburg, Germany*
[3]*Central Laser Facility, STFC Rutherford Appleton Laboratory, Harwell, United Kingdom*
[4]*LUXOR, CNR-INFM, Padova, Italy*
[5]*Diamond Light Source Ltd., Harwell, United Kingdom*
[6]*Institute of Physics of Complex Matter, EPFL, Lausanne, Switzerland*

(Received 8 March 2011; published 18 October 2011)

We use time- and angle-resolved photoemission spectroscopy with sub-30-fs extreme-ultraviolet pulses to map the time- and momentum-dependent electronic structure of photoexcited $1T$-TaS_2. This compound is a two-dimensional Mott insulator with charge-density wave ordering. Charge order, evidenced by splitting between occupied subbands at the Brillouin zone boundary, melts well before the lattice responds. This challenges the view of a charge-density wave caused by electron-phonon coupling and Fermi-surface nesting alone, and suggests that electronic correlations play a key role in driving charge order.

DOI: 10.1103/PhysRevLett.107.177402 PACS numbers: 78.47.jh, 79.60.−i

Charge-density waves (CDWs) underpin the electronic properties of many complex materials [1–4]. The canonical source of CDW order is Fermi-surface nesting, driven by electron-phonon coupling via the Peierls mechanism. In many CDW systems there are also pronounced electron-electron correlations, and with multiple orderings coexisting or competing, it is difficult to tease apart their individual roles in the broken-symmetry phase. Characterizing the interplay between different interaction mechanisms and the associated hierarchy of energy scales and time scales is crucial to understanding CDW physics in real materials.

One family of materials where CDW physics has been widely studied is the layered dichalcogenides, which exhibit a wide diversity of ordered ground states and metal-insulator transitions, providing an ideal playground in which to explore how various ordering processes can cooperate or compete with CDWs. For example, $1T$-$TiSe_2$ may be an excitonic insulator [5], while $1T$-TaS_2 undergoes a Mott transition as it enters a frozen CDW phase [6]. An intriguing superconducting state is also found in the latter compound under pressure [7], hinting at the possibilities for new physics and new devices if these systems can be understood and controlled. The complex nature of these ordered phases, where electron-electron correlations are particularly important, presents an opportunity to explore the limits of the Peierls mechanism as an explanation for CDW order.

In its simplest form, the Peierls mechanism predicts CDW formation in a linear chain of atoms with a half filled valence band and nonzero electron-phonon coupling [8]. A dimer-forming structural distortion will open a gap at the Fermi level, reducing the electronic energy. Distorting the lattice in the presence of electron-phonon coupling must also redistribute charge, and these coupled lattice and charge-density distortions together make up the CDW.

In 1D systems, a CDW can lower the energy of all electrons near the Fermi level, since a single wave vector perfectly connects all electrons on opposite sides of a two-point Fermi surface. In higher dimensions, the same mechanism may operate if large regions of Fermi surface lie parallel to one another, so that they can be connected by a single vector in k space, a condition known as ''nesting.'' This is a rather general effect, in that whenever a coupled boson connects Fermi-surface regions, a static distortion with the symmetry of that boson will insert a new Bragg plane along the nested Fermi surface and open a gap at the Fermi level. The susceptibility therefore diverges at the wavelength of the nesting boson, and a static modulation of the charge or spin density emerges.

Fermi-surface nesting has been widely assumed to play a key role in CDW formation in layered dichalcogenides, but problems with this view are emerging. Many of the Fermi surfaces are not particularly well nested in geometry, and new experimental evidence confirms that the Peierls picture is inadequate or inappropriate in some cases, such as $1T$-$TiSe_2$, where recent time-resolved measurements found that the CDW gap closed on a distinctly electronic time scale [9]. If the gap originated from electron-phonon coupling, one would expect it to close on time scales characteristic of structural distortions, as is the case in 1D CDW systems such as $TbTe_3$ [10]. The

rapid time scale for gap collapse in 1T-$TiSe_2$ thus supports exciton condensation, rather than Fermi-surface nesting, as the cause of CDW formation in that material. In 1T-TaS_2, the gap at the Fermi level is opened by Mott localization due to electron-electron repulsion, with gaps created by the CDW lying below the Fermi level [11]. Here too, then, the Peierls mechanism may be insufficient to explain the CDW phase.

In this work, we use angle-resolved extreme-ultraviolet (XUV) photoemission with 30-fs time resolution to show that in 1T-TaS_2 not only the Mott gap at the Fermi level but also the CDW gaps at finite binding energy melt on subvibrational time scales. This indicates that the CDW gaps close in response to a redistribution of charge, rather than a repositioning of atoms. Electron-electron interactions must therefore lie at the heart of the CDW-induced changes in electronic structure seen in the ordered phase. In other words, correlations play a central role not just in the Mott localization but in CDW formation as well.

At room temperature, 1T-TaS_2 is a metal, exhibiting a nearly commensurate CDW [12,13]. Below 180 K the CDW becomes fully commensurate and locks into the lattice [6,14,15], concomitant with a long-range periodic distortion of the crystal structure [Fig. 1(b)]. This lattice distortion reduces the size of the Brillouin zone and leads to backfolding of the Ta 5d manifold, splitting off several umklapp or ''shadow'' bands [16]. Gaps appear at the new band crossings, and only a narrow band is left at the Fermi level [11,17]. Intracluster Coulomb repulsion further splits that topmost band into Hubbard bands separated by a Mott gap.

In 1T-TaS_2, excitation with ultrashort pulses of light is known to promptly close the Fermi-level gap at the zone center [6], highlighting the importance of Mott physics in the insulating ground state. Photoexcitation also excites the amplitude mode of the CDW [18–20], a 2.4-THz-frequency collective mode in which the star-shaped atomic clusters and the charge density breathe synchronously. Time-resolved electron diffraction experiments [21] show that the long-range atomic-structural order does not completely relax, which is reflected in the low-energy electronic properties of the transient phase [22]. Meanwhile, time-resolved core level photoemission measurements suggest that the on site charge density is already perturbed within 100 fs [23,24], implying that charge and lattice may be decoupled at the earliest time scales.

Optical experiments with subvibrational time resolution [25–28] demonstrate that the nature of a complex insulator is reflected directly in the speed at which its electronic structure rearranges after a prompt change in filling, but optical spectroscopy alone lacks the momentum sensitivity required to fully characterize the transient electronic structure in this material. Instead, it is necessary to measure the time-dependent electronic structure from the center to the boundary of the reduced Brillouin zone, using the various band features as markers of the different forms of electronic order. To do this, we employ ultrafast time- and angle-resolved photoemission.

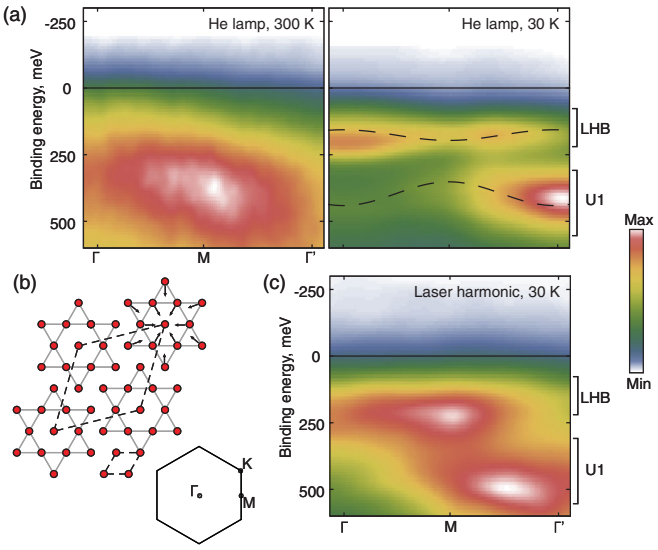

FIG. 1 (color). Structure and ARPES intensity maps of 1T-TaS_2. (a) Static photoemission intensity maps from center to center of the first Brillouin zone, measured with a helium discharge lamp (21.2 eV) at 20 and 300 K. A solid line denotes the Fermi level. Dashed lines indicate the approximate band structure in the low-temperature phase, showing the positions of the LHB (upper band) and U1 (lower band). In both panels, momentum labels refer to the Brillouin zone of the low-temperature structure. (b) Low-temperature lattice distortion in the Ta plane, which accompanies the formation of the commensurate, static CDW. Dashed lines indicate high- and low-temperature unit cells. Gray stars show clusters of atoms formed by the periodic lattice distortion, illustrated by arrows for one star. Also shown is a map of the high-symmetry points of the Brillouin zone. (c) Static intensity map measured with the laser-harmonic XUV source.

In angle-resolved photoemission spectroscopy (ARPES), UV light generates photoelectrons, which are collected and analyzed. Their distribution in energy and angle reveals the occupied states within the material, and therefore the electronic structure [29–31]. Until recently, time-resolved photoemission measurements [6,10] have typically used pulses of 100 fs or longer and only near UV radiation (< 7 eV), making it difficult to access subvibrational time scales and mapping electronic structures over only limited portions of momentum space. To overcome these limitations we use XUV pulses from high-order laser harmonics, with a temporal resolution of 30 fs.

Our measurements employ the time-resolved laser ARPES system at the Artemis facility, in the Central Laser Facility of the Rutherford Appleton Laboratory. A 1-kHz pulsed beam of 30-fs pulses from an amplified 790-nm laser is split into two parts. One stimulates the sample surface with a fluence of approximately 500 $\mu J/cm^2$. The other enters a vacuum beam line, is

focused into a pulsed jet of argon gas, and creates XUV pulses via high-order harmonic generation. These pass through a grating monochromator designed to minimize the pulse length distortion [32], selecting the 13th harmonic (20.4 eV). A grazing-incidence toroidal mirror focuses the pulsed XUV onto the sample, held on a liquid-helium-cooled manipulator in a UHV chamber. Photoelectrons emitted from the surface after each XUV pulse are collected and measured by a hemispherical analyzer. By varying the delay between the infrared and XUV pulses, we follow the electronic structure as a function of time during and after the photoinduced insulator-to-metal transition. The overall energy resolution is approximately 150 meV, limited primarily by the line width of the laser XUV source. Improving this energy resolution would sacrifice time resolution. Samples are cleaved under UHV while cold, and surface quality is inspected by LEED before and after ARPES runs.

Figure 1(a) shows static photoemission intensity maps indicating the band structure near the Fermi level E_F taken with an ultraviolet helium lamp below and above the thermal phase transition at 180 K. At low temperatures, reduced photoemission intensity at the Fermi energy indicates the opening of the Mott gap. The band immediately below E_F is the lower Hubbard band (LHB). A gap between subbands is evident at the reduced Brillouin zone boundary (the M point). High-momentum states are folded back into the first (reduced) zone, so the split-off bands reappear as umklapp bands at $k = 0$ (the Γ point). We call the uppermost of these U1. Each of these features is captured in the static photoemission intensity map obtained with our laser-based XUV source in Fig. 1(c). The quantitative differences between the two static spectra arise from the differences between the sources: the He lamp is not polarized while the high-order harmonic source is p polarized, and the photon energies are slightly different.

Figure 2 shows the energy distribution of intensity at the Γ and M points as a function of time after photostimulation by a pulse of 790-nm light. At Γ, a rapid loss of intensity in the LHB confirms that the Mott gap collapses, accompanied by filling in of states at and above the Fermi level. This is followed by recovery of the original peak, followed by a rigid oscillation of the band edge at the frequency of the CDW amplitude mode. These observations are in accord with earlier results [6], where 6-eV photon energy pulses were used to study states near $k = 0$. At the M point, there is a similar rapid loss of overall intensity, transfer across E_F, and recovery. In addition, the splitting between U1 and LHB is destroyed, as is visible in the individual energy spectra of Fig. 2(b), where the distinct peaks of the LHB and U1 bands, divided by an umklapp gap, merge into a single feature. These prompt changes are followed by the rapid recovery of both gaps. The entire LHB-U1 complex then oscillates at the frequency of the CDW amplitude mode.

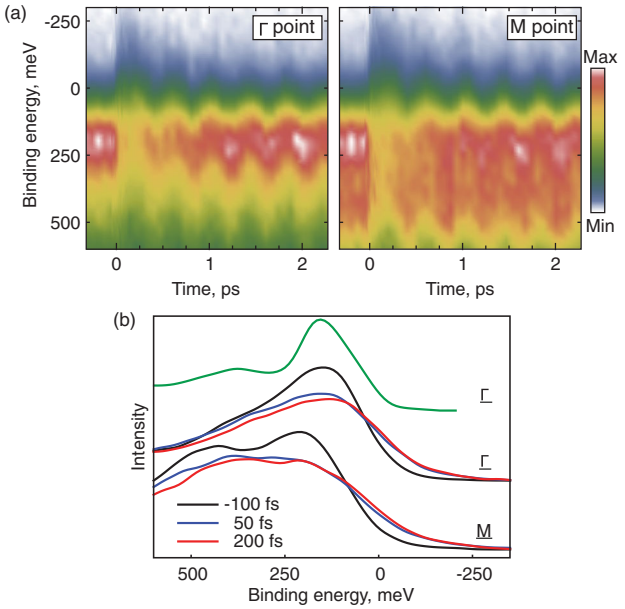

FIG. 2 (color). Collapse of the Mott and CDW gaps and oscillation of the LHB edge. (a) Maps of photoelectron intensity as a function of time, during and after photoexcitation. At both the Γ and M points, a transfer of intensity across the Fermi level at $t = 0$ heralds the prompt destruction of the Mott gap. Mott gap recovery, after a few hundred fs, is followed by a rigid oscillation at the amplitude-mode frequency. (b) Individual energy distribution curves before and after photoexcitation. Along with the loss of the Mott gap, which causes intensity to drop in the LHB and be transferred to energies around and above the Fermi level, there is also a rapid loss of splitting between the band features at the M point. The top curve (green) is a reference measurement taken with a lamp source, showing the two bands at the zone center.

Next, we consider the detailed dynamics and k dependence of the changes in the LHB and U1 bands during the formation of the photometallic phase. The destruction of both gaps is clearly evident on subvibrational time scales. Figure 3 shows maps of the photoemission intensity at various times during the ultrafast phase transition. Again, intensity is lost at the peak of the LHB and transferred across the Fermi level as a result of the melting of the Mott state. Simultaneously, the gap between subbands disappears at the M point, indicating that the CDW order has melted as well. However, not all changes to the electronic structure proceed so promptly. Figure 4(a) shows a more detailed examination of the time dependence at Γ. At the Fermi level, where the increase in intensity corresponds to the collapse of the Mott gap, the change is expected to proceed on the time scale of hopping [27]. The transition here is effectively prompt, occurring on a time scale faster than the 30-fs resolution of the experiment. The same process drives the initial changes at the peak of the LHB, which also rearranges promptly.

In contrast to the prompt loss of the U1-LHB splitting, at the lower energies of the U1 band at Γ the response is

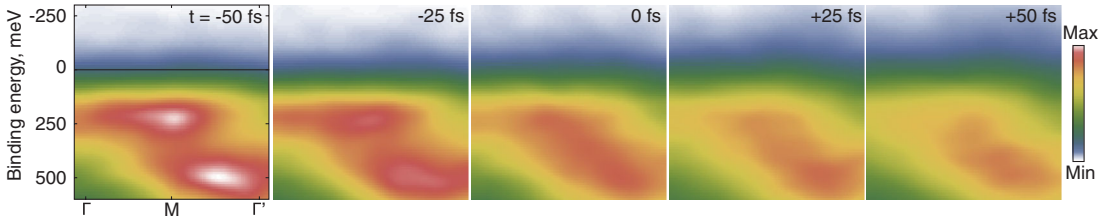

FIG. 3 (color). Snapshots of momentum-dependent photoemission intensity, obtained with the laser-harmonic XUV source at 20 K. As the insulator-metal transition proceeds, transfer of intensity across the Fermi level is evident throughout both Brillouin zones. The gap between bands at the zone boundary collapses on subvibrational time scales.

slower, well described by a transient response with a time scale of a half-cycle of the amplitude mode. This is consistent with a reduction in spectral weight in the umklapp band brought about by relaxation of the lattice distortion, which proceeds on structural rather than electronic time scales [21].

To illustrate this idea further, Fig. 4(b) shows the changes in intensity across the entire range of momenta. The first panel shows the relative changes from 50 fs before photoexcitation to 50 fs after, while the second panel shows the changes between 50 and 200 fs after photoexcitation. The changes on short time scales reiterate that at early times there is a loss of intensity in each band, but particularly at the peak of the LHB, and a gain in intensity at the Fermi level and above as a consequence of photoinduced melting of the Mott state and the creation of hot electrons. This process is largely independent of momentum, indicating that the effects of electron-electron interaction pervade the Brillouin zone.

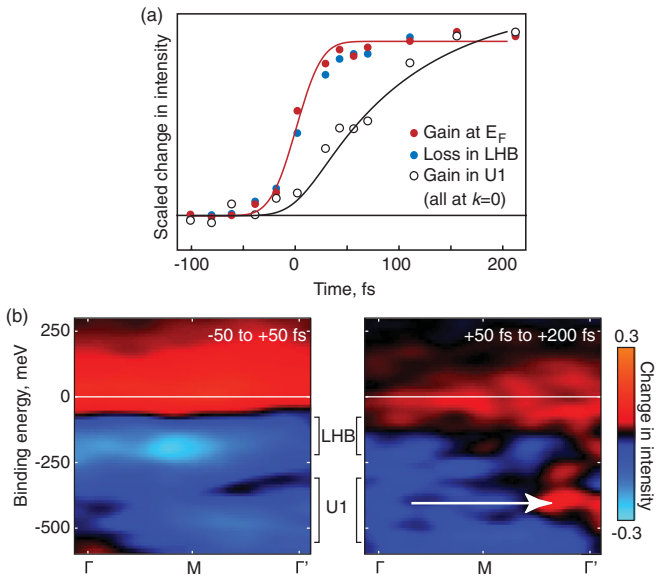

FIG. 4 (color). Momentum dependence of spectral changes on fast and slow time scales. (a) Time evolution at the Γ point, scaled, for three key energies. Changes are prompt in the lower Hubbard band and at E_F, but much slower in the umklapp band (U1). Red and black curves show a step response and a transient response with a lifetime of half the amplitude-mode period, each convolved with the instrumental resolution. (b) Maps of intensity changes. The first panel shows immediate changes, between −50 and +50 fs. The second panel shows the subsequent change, between +50 and +200 fs. All changes are expressed relative to the peak intensity before photostimulation. The arrow indicates the unfolding of intensity out of the first reconstructed Brillouin zone as the structural distortion begins to relax.

More dispersive electronic structural changes are seen at longer time delays, and two key features are apparent. Intensity is lost in U1 bands at Γ, with this intensity reappearing at Γ′, the image of Γ reflected across the reconstructed zone boundary. This provides a direct snapshot of the unfolding of the Brillouin zone as the structural distortion begins to relax. Overall, intensity is lost below the LHB peak and gained above it, indicating that the band edge is moving upward as the structure begins to relax.

The fact that these different processes take place on distinctly electronic and structural time scales gives new information about both the static band structure of 2D CDW materials and the process by which they melt after ultrafast excitation. To explain this rapid closing of the zone-boundary gap, we must conclude that the CDW order is lost on subvibrational time scales, and that the zone-boundary gaps reflect the broken symmetry of charge density in the CDW ground state. On the other hand, the intensity of the shadow bands at the zone center must be a manifestation of the periodic lattice distortion. Thus the CDW melts via prompt destruction of the charge order, to which the lattice then responds on its own time scale by relaxation of the periodic lattice distortion. Previous experiments have shown rapid melting of a CDW gap [9] in some systems and slow melting of lattice order [21] in others, but this is the first time that multiple time scales for different electronic-structural features have been observed in one material in a single measurement.

In summary, time-resolved ARPES with XUV radiation allows us to study the relaxation of a charge-density wave in photostimulated 1T-TaS_2, measuring charge order at the edge of the reconstructed Brillouin zone with subvibrational time resolution. By clocking the evolution of various changes, we assign specific features of the electronic structure to individual aspects of the ordered ground state. The gaps in the zone-boundary spectral function originate from the charge-density ordering, which melts promptly

after photostimulation. Subsequently, spectral intensity migrates from shadow bands in the first zone back out to higher momentum, revealing the unfolding of the Brillouin zone that accompanies incipient lattice relaxation along the coordinate of the Raman active amplitude mode following photodoping [21]. At longer time scales, charge order and lattice distortions lock again, displaying the well-known modulations of spectral weight at the frequency of the amplitude mode.

This hierarchy of time scales indicates that charge and lattice order must decouple at early times, so that it will clearly be necessary to go beyond the phase- and amplitude-mode picture of CDW dynamics [8] to understand this system. An electronic origin for the umklapp gaps also casts into doubt the dominant conception of the thermal phase transition as being primarily driven by nesting with Mott physics following. Instead, electronic correlations seem to play a much more central part in the CDW ordering itself.

We thank S. Hook and T. Strange for technical support, and C. Froud and W. A. Bryan for assistance with the development of the beam line. This research received funding from the EC Seventh Framework programme via Laserlab Europe.

[1] F. Clerc *et al.*, J. Phys. Condens. Matter **16**, 3271 (2004).
[2] M. Grioni, L. Perfetti, and H. Berger, J. Electron Spectrosc. Relat. Phenom. **137–140**, 417 (2004).
[3] G. H. Gweon *et al.*, J. Electron Spectrosc. Relat. Phenom. **117–118**, 481 (2001).
[4] D. Jérome and H. J. Schulz, Adv. Phys. **31**, 299 (1982).
[5] H. Cercellier *et al.*, Phys. Rev. Lett. **99**, 146403 (2007).
[6] L. Perfetti *et al.*, Phys. Rev. Lett. **97**, 067402 (2006).
[7] B. Sipos *et al.*, Nature Mater. **7**, 960 (2008).
[8] G. Grüner, *Density Waves in Solids* (Perseus, Cambridge, MA, 2004).
[9] T. Rohwer *et al.*, Nature (London) **471**, 490 (2011).
[10] F. Schmitt *et al.*, Science **321**, 1649 (2008).
[11] K. Rossnagel and N. V. Smith, Phys. Rev. B **73**, 073106 (2006).
[12] J. A. Wilson, F. J. DiSalvo, and S. Mahajan, Adv. Phys. **24**, 117 (1975).
[13] P. Fazekas and E. Tosatti, Philos. Mag. B **39**, 229 (1979).
[14] F. Clerc *et al.*, Phys. Rev. B **74**, 155114 (2006).
[15] L. V. Gasparov *et al.*, Phys. Rev. B **66**, 094301 (2002).
[16] L. Perfetti *et al.*, Phys. Rev. B **71**, 153101 (2005).
[17] M. Arita *et al.*, Physica (Amsterdam) **351B**, 265 (2004).
[18] J. Demsar *et al.*, Phys. Rev. B **66**, 041101(R) (2002).
[19] L. Perfetti *et al.*, New J. Phys. **10**, 053019 (2008).
[20] R. Yusupov *et al.*, Nature Phys. **6**, 681 (2010).
[21] M. Eichberger *et al.*, Nature (London) **468**, 799 (2010).
[22] N. Dean *et al.*, Phys. Rev. Lett. **106**, 016401 (2011).
[23] S. Hellmann *et al.*, Phys. Rev. Lett. **105**, 187401 (2010).
[24] K. Ishizaka *et al.*, Phys. Rev. B **83**, 081104(R) (2011).
[25] A. Cavalleri *et al.*, Phys. Rev. B **70**, 161102 (2004).
[26] D. Polli *et al.*, Nature Mater. **6**, 643 (2007).
[27] S. Wall *et al.*, Nature Phys. **7**, 114 (2010).
[28] S. Wall *et al.*, Phys. Rev. Lett. **103**, 097402 (2009).
[29] Z. X. Shen and D. Dessau, Phys. Rep. **253**, 1 (1995).
[30] A. Damascelli, Z. Hussain, and Z. X. Shen, Rev. Mod. Phys. **75**, 473 (2003).
[31] J. Koralek *et al.*, Phys. Rev. Lett. **96**, 017005 (2006).
[32] F. Frassetto *et al.*, Proc. SPIE Int. Soc. Opt. Eng. **7077**, 707713 (2008).